Materials Science & Engineering C 93 (2018) 539–553

Contents lists available at ScienceDirect

Materials Science & Engineering C

journal homepage: www.elsevier.com/locate/msec

Evaluation of the corrosion inhibiting efficacy of a newly synthesized nitrone against St37 steel corrosion in acidic medium: Experimental and theoretical approaches

Hüsnü Gerengi[a], Moses M. Solomon[b,*], Serkan Öztürk[c], Ayhan Yıldırım[c], Gökhan Gece[d], Ertuğrul Kaya[a]

[a] Corrosion Research Laboratory, Department of Mechanical Engineering, Faculty of Engineering, Düzce University, 81620 Düzce, Turkey
[b] Centre of Research Excellence in Corrosion, Research Institute, King Fahd University of Petroleum and Minerals, Dhahran 31261, Saudi Arabia
[c] Department of Chemistry, Faculty of Science and Arts, Uludağ University, 16059 Bursa, Turkey
[d] Department of Chemistry, Faculty of Engineering and Natural Sciences, Bursa Technical University, 16310 Bursa, Turkey

ARTICLE INFO

Keywords:
Steel
Acid corrosion
Corrosion inhibitor
Organic compounds
Amphiphilic nitrone

ABSTRACT

A novel amphiphilic nitrone, *N*-phenyl-1-(4-((11-(pyridin-1-ium-1yl) undecanoyl) oxy)phenyl)methanimine oxide bromide (NP-1-4-11-PUOPMOB) has been synthesized from a fatty acid derivative as a starting material. Structural characterization of the new compound has been realized by spectroscopic techniques (FTIR, ^{1}H NMR, and ^{13}C NMR). The corrosion inhibition effect of the compound for St37 steel corrosion in 1 M HCl medium has been investigated using experimental (weight loss, electrochemical impedance spectroscopy, potentiodynamic polarization, dynamic electrochemical impedance spectroscopy) and theoretical approaches complemented by surface morphological examination using energy dispersive X-ray spectroscopy, scanning electron microscope, and atomic force spectroscopy. Results from both chemical and electrochemical techniques reveal that the presence of the nitrone in the acid solution impedes St37 steel corrosion. The inhibition efficiency obtained at 125 ppm and 150 ppm concentrations for all methods is found to be over 90%. NP-1-4-11-PUOPMOB behaves as a mixed type corrosion inhibitor according to the potentiodynamic polarization studies. The adsorption of NP-1-4-11-PUOPMOB molecules onto the metal surface follows Langmuir adsorption isotherm and the calculated K_{ads} (equilibrium constant of the adsorption process) value reflects strong interaction. There is evidence of NP-1-4-11-PUOPMOB adsorption on the metal surface from SEM, EDAX, and AFM studies. Experimental and theoretical results are in good agreement.

1. Introduction

In the oil and gas industry, steel is largely utilized for diverse applications such as fluid transportation line, storage tank, and drilling pipe [1,2]. In many cases, industrial practices like mill scale removal, acid cleaning, oil well acidizing, etc. bring metals in contact with corrosive solutions. It is therefore a common practice to add corrosion inhibitors into corrosive solutions before metal pre-treatment [3–6].

In corrosion studies, there are several methods (weight loss (WL), potentiodynamic polarization (PDP), electrochemical impedance spectroscopy (EIS), etc.) used to determine the effectiveness of a corrosion inhibitor. Even in recent years, there are many studies in the literature that used these methods together [7–11]. The electrochemical impedance spectroscopy (EIS) technique is very versatile and is noted for its ability to provide information on the mechanism and corrosion kinetics of metals in a corrosive environment [12]. Three cardinal conditions of linearity, casuality, and stationary state must be satisfied for accurate measurement with EIS [12]. In practice, the first two conditions can now be met easily but the third condition is somewhat impossible since corrosion process is dynamic in nature [12]. This constitutes a setback to the use of EIS in corrosion studies. Dynamic electrochemical impedance spectroscopy (DEIS) is considered as a new method for corrosion studies and is a modified version of EIS that involves the application of Short-Time Fourier Transform (STFT) coupled with multi-sinusoid perturbation signal in corrosion measurement. The DEIS technique allows the measurement of corrosion processes on a metal surface in a non-stationary system [12]. This technique has been used in several corrosion studies [13–16] and the results compare

* Corresponding author.
E-mail address: moses.solomon@kfupm.edu.sa (M.M. Solomon).

https://doi.org/10.1016/j.msec.2018.08.031
Received 6 March 2018; Received in revised form 5 July 2018; Accepted 11 August 2018
Available online 13 August 2018
0928-4931/

Table 1
Previous studies on organic compounds with pyridinium moiety as corrosion inhibitors.

Organic compound	Corrosive medium	Metal substrate	Method(s)[a]	Max. inhibition efficiency (%)	Ref.
Cetyl pyridinium chloride	H_3PO_4	Low carbon steel	WL	90 at 30 °C	[17]
N-alkyl-2-(4-hydroxybut-2-ynyl)pyridinium bromide	HCl	X70 steel	WL, EIS, PDP, XPS	97 from EIS at 30 °C	[18]
1-Dodecyl/tetradecyl/hexadecyl-3-(4-hydroxybut-2-ynyl)pyridinium bromide	HCl	X70 steel	WL, EIS, PDP, SEM	98 from EIS at 30 °C	[19]
N-octadecyl pyridinium bromide	H_2SO_4	Mild steel	PDP, SEM, EDX	97 from EIS at 25 °C	[20]
N-alkyl-4-(4-hydroxybut-2-ynyl)pyridinium bromide	HCl	X70 steel	WL, EIS, PDP, SEM	97 from EIS at 30 °C	[21]
N-cetyl-3-(2-methoxycarbonyl vinyl)pyridinium bromide	HCl	X70 steel	WL, EIS, PDP, SEM, EDX	96 from EIS at 30 °C	[22]
N-alkyl-3-(2-methoxycarbonyl-vinyl)pyridinium bromide	HCl	X70 steel	WL, EIS, PDP, Quantum chemical calculations	96 from EIS at 30 °C	[23]
Hexadecyl pyridinium bromide	HCl; H_2SO_4	Fe; Cu	PDP	98 in HCl; 82 in H_2SO_4	[24]
	H_2SO_4	Mild steel	WL, PDP	97 from WL at 60 °C	[25]
	H_2SO_4	Stainless steel (SS304L, SS316L, SS304H)	EIS, PDP, AC impedance	78–91 from PDP at 25 °C	[26]
1-Methyl-4[4′(-X)-styryl pyridinium iodide (X = −H, $-CH_3$, or $-OCH_3$)	HCl	Mild steel	WL, HE	96–99 from WL at 25 °C	[27]

[a] WL = weight loss; EIS = electrochemical impedance spectroscopy; PDP = potentiodynamic polarization; SEM = scanning electron microscope; XPS = X-ray photoelectron spectroscopy; EDX = energy dispersive X-ray spectroscopy; HE = hydrogen evolution.

favourably with the results of other techniques.

A survey of the corrosion literature (Table 1) reveals that organic compounds with pyridinium moiety demonstrate favorable corrosion inhibition [17–27], and typically cationic surfactants containing heteroatoms such as O, N, S and P are highly effective corrosion inhibitors in acidic media [28–32]. The hydrocarbon part of these molecules plays a significant role in inhibition. Depending on the length of the hydrocarbon chain non-polar van der Waals interactions provide better barrier against aggressive environments. Although many organic corrosion inhibitors are known in the literature, study on the corrosion inhibition properties of nitrones is far less [33–35]. In addition, no study has been undertaken on the corrosion inhibition by amphiphilic nitrones to the best of our knowledge. As it is known [36], amphiphilic compounds possess both hydrophilic and lipophilic properties, and accordingly, these compounds act as a surfactant in both aqueous and organic (polar or non-polar) solutions. Durand et al. [37] had reported that amphiphilic amide nitrones besides being a radical scavenging antioxidant can also act as a bioenergetic agent directly on mitochondrial electron and proton transport.

In the present study, the inhibition efficiency of a newly synthesized organic compound with pyridinium moiety, *N*-phenyl-1-(4-((11-(pyridin-1-ium-1yl) undecanoyl) oxy)phenyl)methanimine oxide bromide (NP-1-4-11-PUOPMOB) (Fig. 1) for St37 steel corrosion in 1 M HCl solution has been examined using WL, EIS, PDP, and DEIS complemented with surface assessment using energy dispersive X-ray spectroscopy (EDAX), scanning electron microscope (SEM), and atomic force spectroscopy (AFM). Theoretical calculations have also been performed on this compound by density functional theory (DFT) approach to substantiate the experimental results.

No studies have been conducted on biodegradation of the inhibitor; however, the compound is prepared from renewable and biodegradable starting compounds. Biodegradation of organic compounds such as surface active substances is dependent not only on the environmental conditions but also on the molecular structures of the compounds [38].

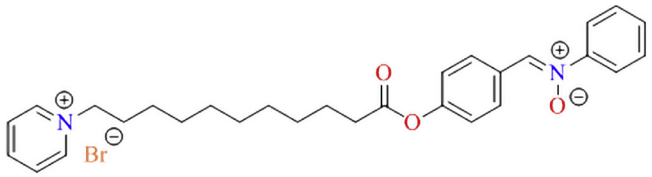

Fig. 1. Molecular structure of NP-1-4-11-PUOPMOB.

In this work, the ester functional group is present in the structure of the synthesized inhibitor compound, and as is known, this group is easily biodegradable [39]. Therefore, biodegradation of the inhibitor compound is facilitated after the hydrolysis of ester functional group. In other words, the molecule is divided into fragments and biodegradation accelerates. This justifies our motivation to synthesize this compound and to use it as a corrosion inhibitor.

2. Experimental

2.1. Materials, solutions and instrumentation

A St37–2 steel sheet (St37 is however used in the text for convenience) was acquired from Erdemir Steel Company, Turkey. The metal has the following chemical composition (wt%): C 0.17, Mn 1.40, P 0.05, Si 0.30, S 0.05, and the balance Fe [14]. Specimens used in corrosion studies were prepared from the St37 steel sheet. The coupons were cut into a rectangular shape of 0.1 × 2.2 × 5.0 cm in thickness, width and length, respectively for the gravimetric measurements. The specimens used for electrochemical experiments were cylindrical in shape with 0.75 cm^2 as the exposed surface area. Before use, the specimens were mechanically abraded with emery papers down to 2000 grit. Thereafter, they were degreased in acetone, rinsed with ethanol and dried in warm air flow (the temperature of the warm air stream is about 40 °C) [40].

All reagents and solvents, namely, acetonitrile (CH_3CN, 99.8%), diethyl ether ($(CH_3CH_2)_3O$, ≥99.7%), pyridine (C_5H_5N, ≥99.0%), ethanol (CH_3CH_2OH, ≥99.8%), methanol (CH_3OH, ≥99.9%), β-phenylhydroxylamine (C_6H_7NO, ≥97.0%), and hydrochloric acid (HCl, 37%) were purchased from either Merck or Sigma-Aldrich and used without further purification. Thin layer chromatography (TLC) was performed using silica gel (60 F254, Merck, Darmstadt, Germany) plates. Melting points were recorded using a BUCHI melting point B-540 (BUCHI Labortechnik AG in Flawil, Switzerland) apparatus. NUVE EV 018 vacuum oven was used to dry the metal coupons to a constant weight except from the atmospheric air. Nicolet FT–IR 6700 spectrometer (Thermo Fisher Scientific Inc., Waltham, MA, USA) was used for the FT–IR spectra. ^1H NMR and ^{13}C NMR spectra were measured using Agilent 600 MHz Premium Compact NMR spectrometer in DMSO-d_6 using TMS as the internal standard. Chemical shifts (δ) are reported in ppm and J values in Hertz. The AFM images were taken with Ambient AFM/MFM (Nanomagnetics Instruments, Oxford, UK).

2.2. Synthesis of compounds

2.2.1. Synthesis of 1-(11-(4-formylphenoxy)-11-oxoundecyl)pyridin-1-ium bromide, (2)

Aldehyde, **1** [41] (3 g, 8.12 mmol), pyridine (0.7 g, 8.85 mmol) and 15 mL of acetonitrile as solvent were placed in a 100 mL flask fitted with a reflux condenser. The reaction mixture was refluxed for 24 h and then the solvent was removed under reduced pressure. Thereafter the residue was dissolved in minimum amount of methanol (MeOH) and washed several times with large amounts of diethyl ether that was discarded in each case. Upon violent agitation the solidifying beige product (**2**) was filtered under vacuum and washed several times with diethyl ether. Yield 3.5 g, 96%, mp: 64–66 °C.

2.2.2. Synthesis of N-phenyl-1-(4-((11-(pyridin-1-ium-1yl) undecanoyl) oxy)phenyl)methanimine oxide bromide, (3)

In a 50 mL flask aldehyde **2** (3 g, 6.69 mmol) and β-phenylhydroxylamine (0.89 g, 8.16 mmol) were dissolved in 10 mL of ethanol (EtOH). The flask was sealed and allowed to stand for 48 h in the dark. Thereafter the obtained beige crystals were filtered under vacuum and washed with diethyl ether to afford **3**. Yield 3.2 g, 89%, mp: 119–121 °C.

2.3. Corrosion tests in acidic media

2.3.1. Weight loss measurements

The weight loss corrosion tests in 1.0 M HCl solution were carried out in accordance with the relevant standard method [42]. Inhibition efficiencies of the synthesized cationic nitrone compound were tested at different concentrations in 100 mL 1.0 M HCl solution. Specifically, 25, 50, 100, 125, and 150 ppm by mass of NP-1-4-11-PUOPMOB were utilized in the corrosion inhibition studies. The cationic nitrone compound was directly dissolved in the acid solution. Afterwards, the treatment solutions were poured into 150 mL sealed glass bottles, and the coupons were suspended in these solutions without stirring for 24 h at room temperature. Control test was performed in the same way in the absence of the inhibitor. After the corrosion test, the coupons were removed, washed with distilled water and acetone and then dried with warm air (air temperature was about 40 °C) [28,29].

2.3.2. Dynamic electrochemical impedance spectroscopy (DEIS)

The DEIS experiments were performed using a frequency response analyzer (FRA) which has a galvanostat model. A National Instruments Ltd. PCI-4461 digital-analogue card was used to generate current perturbation [15]. The card was also used to record the current and voltage signals. The sampling frequency was 12.8 kHz and the perturbation signal was a package comprising of current sinusoids of the frequency range from 4.5 kHz to 700 MHz.

2.3.3. Electrochemical impedance spectroscopy (EIS) and potentiodynamic polarization (PDP)

A Reference 600 Gamry instrument was used for this set of experiments. The instrument is built with DC105 and EIS300 softwares for PDP and EIS experiments respectively. The working electrode was the prepared St37 having exposed area of 0.75 cm^2. A Ag/AgCl electrode performed the function of a reference electrode while the counter electrode was a Pt plate. As required by the principles governing EIS, the working electrode was retained in test solutions for 7200 s for the purpose of achieving a stable open circuit potential (OCP) (Fig. 2). All the electrochemical corrosion experiments were repeated for a reasonable number of times under the same conditions to ensure that the results are reproducible.

For the PDP experiments, the metal substrate was scanned at a rate of 1 mV/s at −250 to +250 mV interval relative to corrosion potential (E_{corr}). The linear parts of the anodic and cathodic branches of the polarization curves were extrapolated to derive the polarization parameters associated with the corrosion process. The EIS measurements were conducted at E_{corr} using an amplitude signal of 10 mV peak-to-peak in the frequency range of 10 mHz to100 kHz. For the analysis of EIS spectra, ZSimWin 3.22 program was used.

2.4. Surface screening

Metal coupons (St37 steel samples) which were cut into a square shape of 0.1 × 2.0 × 2.0 cm thickness, width and length, respectively were used for the surface screening techniques. Coupons were abraded with various grit of emery paper (#400–#2000) to mirror surfaces, washed with acetone, and then dried with warm air (air temperature was about 40 °C). The prepared steel coupons were exposed to 1 M HCl solutions with and without NP-1-4-11-PUOPMOB for 24 h at room temperature. After immersion time of 24 h, the steel specimens were retrieved and dried at room temperature. The surface was then screened using a Carl Zeiss EVO 40 (SEM). All SEM images were taken at a magnification power of 1000×. For the AFM surface roughness determination, specimens were prepared same way as for SEM samples except that, they were gently washed in running water and acetone and dried in warm air after retrieving from test solutions before submitting for the analysis. AFM analysis was performed using an Ambient AFM/MFM (Nanomagnetics Instruments, Oxford, UK) model atomic force microscope. An electron dispersive X-ray spectroscopy (EDAX) detector was used for elemental compositional analysis of the metal samples before and after exposure to test solutions.

2.5. Quantum chemical calculations

All density functional theory (DFT) calculations were carried out with the 6–311 + + G(d,p), a triple-ζ basis set augmented with polarization and diffuse functions in Gaussian 09 package [43–45], where SCF calculations failed to converge using default run parameters, the keyword Integral = (Acc2E = 12) was used to increase the two-electron integral accuracy. B3LYP functional was selected based on previously assessed performance for noncovalent interactions [46], and the calculated geometries showed no imaginary frequencies. Molecular properties were deduced from HOMO − LUMO analysis in the gas and aqueous phases within the integral equation formalism-polarizable continuum model (IEF-PCM) with water as the solvent.

3. Results and discussion

3.1. Chemical synthesis

An amphiphilic nitrone compound was synthesized as potential corrosion inhibitor for St37 steel in acidic media. The synthetic pathway for the preparation of the amphiphilic nitrone is shown in Scheme 1.

As seen from Scheme 1, the starting long chained compound **1** [41] was refluxed with pyridine in acetonitrile for 24 h to obtain the cationic pyridinium derivative **2**. In the second step, pyridinium derivative **2** was reacted with *N*-phenylhydroxylamine in ethanol for 48 h at room temperature to afford the amphiphilic nitrone **3** in fairly good yield. The structures of the novel compounds **2** and **3** were confirmed by FT-IR, ^{1}H NMR and ^{13}C NMR spectroscopic methods. The spectra and spectral characterization data of the synthesized compounds are given in Figs. 3 & 4 and Table 2.

The IR spectrum of starting compound **2** exhibits intense bands at 1757, 1690 and 1634 cm^{-1} due to stretch of ester carbonyl group (C═O), aldehyde carbonyl group (C═O) and pyridine (C═N^+) group, respectively. Compound **3** shows characteristic bands at 1754, 1636, 1551 and 1067 cm^{-1} which is associated with the stretch of ester carbonyl group (C═O), pyridine (C═N^+) group, nitrone group (C═N) and nitrone (N−O) group, respectively. The evaluation of ^{1}H NMR spectrum of the synthesized precursor aldehyde **2**, showed that −C<u>H</u>O

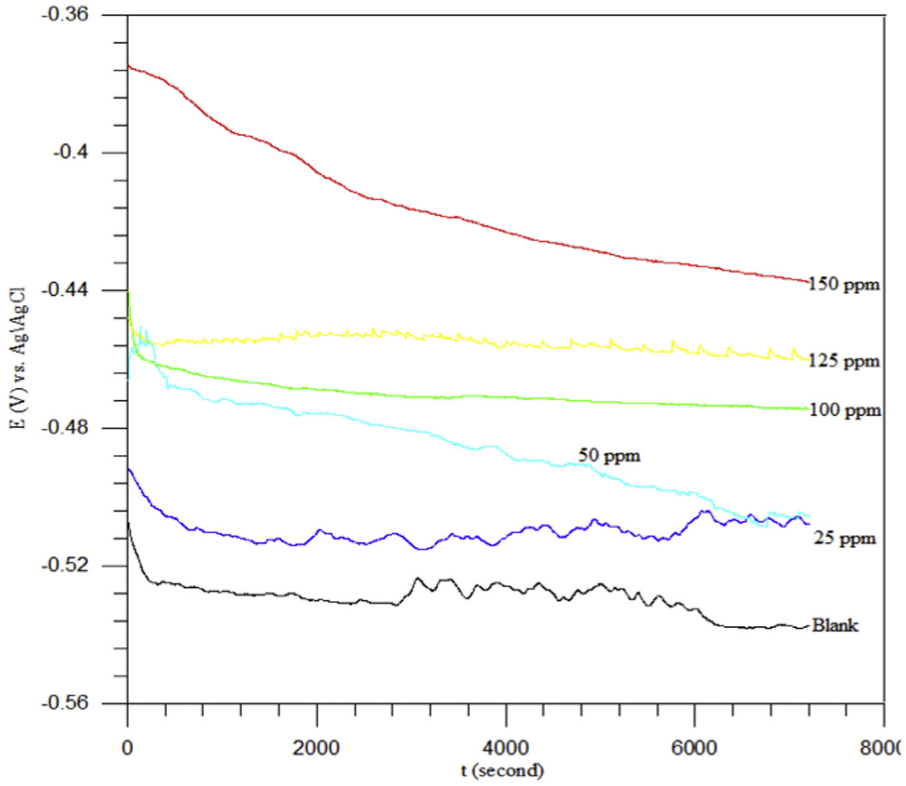

Fig. 2. E_{OCP} versus time curves for St37 steel in 1 M HCl solution at 25 °C in absence and presence of different concentrations of NP-1-4-11-PUOPMOB.

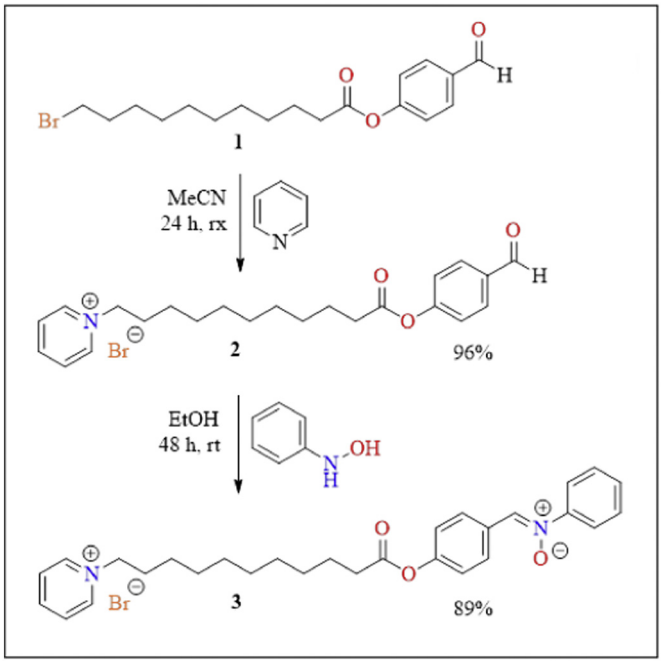

Scheme 1. Synthetic pathways for the preparation of amphiphilic nitrone **3**.

carbonyl proton has a chemical shift of 9.98 ppm; methylene protons next to pyridine ring N atom have a chemical shift of 4.60 ppm as a triplet peak and methylene protons next to ester carbonyl group have chemical shift of 2.59 ppm as a triplet peak, which are the basic characteristic peaks of this compound. On the other hand, ^{1}H NMR spectrum of the inhibitor nitrone compound **3**, showed peaks at 7.55–7.49 ppm as a multiplet and 7.24 ppm as a doublet belonging to aromatic ring protons next to the N atom of nitrone functionality. Additionally, the ^{13}C NMR spectrum of the compound **2** confirmed the proposed structure, peaks at 192.46 ppm and 171.82 ppm belong to C atoms of aldehyde and ester carbonyl groups, respectively. In the ^{13}C NMR spectrum of the compound **3**, the peak of C atom belongs to nitrone moiety appeared at 148.82 ppm.

3.2. Corrosion tests in acidic media

3.2.1. Weight loss measurements

The results from the corrosion tests in acidic media (1 M HCl) which were performed using weight loss measurements are given in Table 3. Percentage inhibition efficiency (η) was calculated using Eq. (1) as follows:

$$\eta_{WL} = \frac{W_0 - W}{W_0} \times 100 \quad (1)$$

where W_0 is the weight loss of the coupon in the absence of an inhibitor and W is the weight loss of the coupon in the same environment in the presence of an inhibitor. The corrosion rate (ν) values were derived from Eq. (2) [47]:

$$\nu = \frac{\Delta W}{At} \quad (2)$$

where ΔW is the weight loss (mg); A is the area of the coupon (cm^2) and t is the immersion time (h).

As shown in Table 3, the cationic amphiphilic nitrone compound exhibited good corrosion inhibition in studied inhibitor concentrations. The weight loss and corrosion rate decrease while inhibition efficiency increases with increasing inhibitor concentration. Corrosion rate as low as 0.0088 ($mg\ cm^{-2}\ h^{-1}$) and high inhibition efficiency of 94.84% was achieved with inhibitor concentration of 150 ppm. The measured corrosion rates in the presence of inhibitor are seen to be significantly lower than that of the inhibitor-free acid solution. This results portray NP-1-4-11-PUOPMOB as effective corrosion inhibitor for steel in the acid simulating pickling bath.

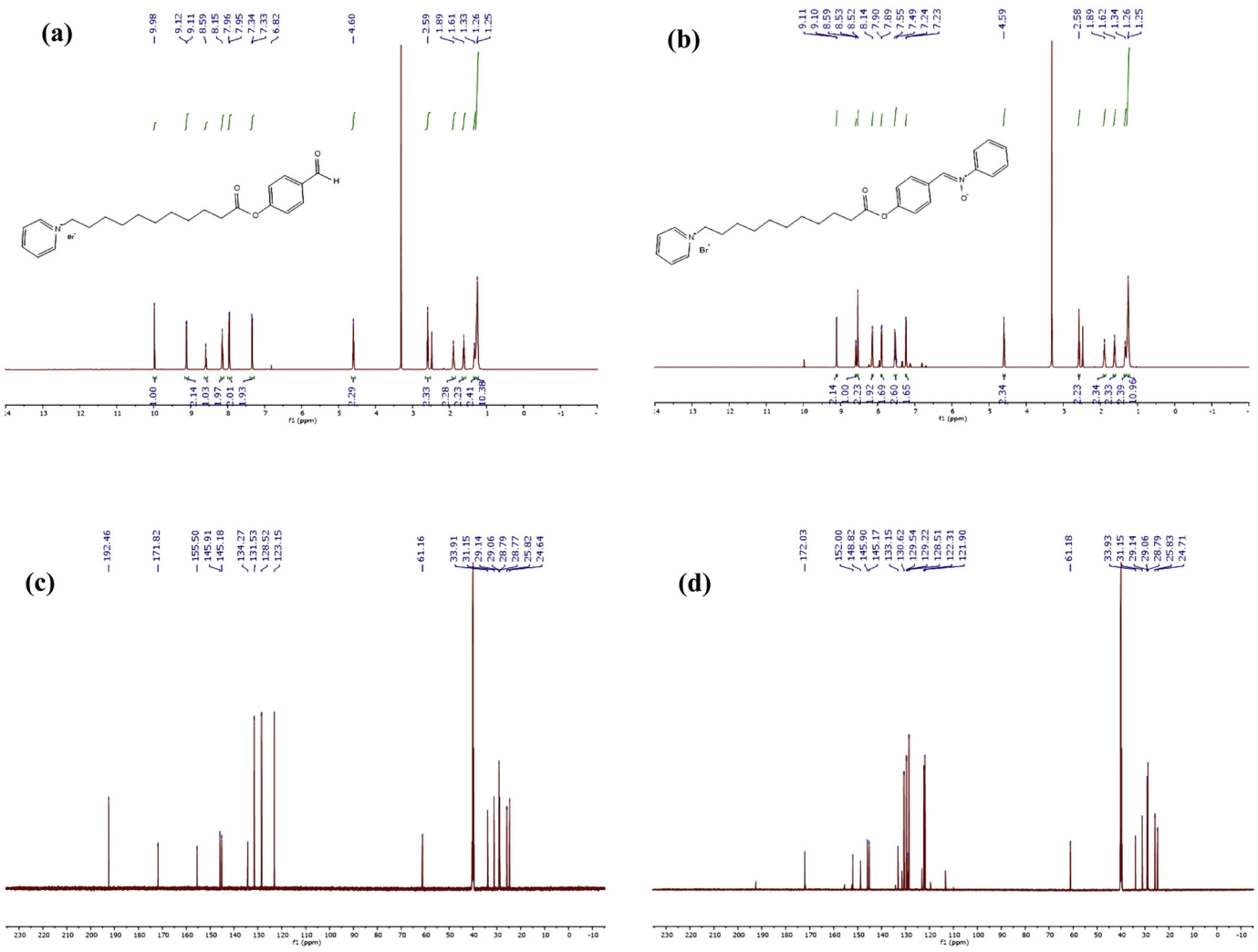

Fig. 3. ^{1}H NMR spectrum of (a) compound **2** and (b) compound **3**; ^{13}C NMR spectrum of (c) compound **2** and (d) compound **3**.

3.2.2. Electrochemical measurements

3.2.2.1. DEIS studies. DEIS technique is a modified EIS method with the ability to track changes on a metal surface in a non-stationary system [15] (EIS requires stationary environment for accurate measurements). Fig. 5 shows the DEIS spectra obtained for St37 steel in 1 M HCl solution containing 25 ppm and 150 ppm NP-1-4-11-PUOPMOB respectively at various times of measurements in Bode modulus format. The influence of the inhibitor on the corrosion behaviour of the metal specimen can be clearly seen in Fig. 5. The impedance is displaced toward nobler direction on introduction of inhibitor into the corrosive system (Note: NP-1-4-11-PUOPMOB was added to the system after 30 min of commencement of experiment) and may be reflective of corrosion inhibition. The impedance seems near constant with increase in measurement time.

To gain insight into the influence of NP-1-4-11-PUOPMOB on the charge transfer process, a plot of charge transfer resistance (R_{ct}) against immersion time (s) is drawn (Fig. 6). Interestingly, the R_{ct} vs t graph for the blank solution appears near constant throughout the time of measurement suggesting an unperturbed dissolution process of St37 steel in the environment. Compared with the graphs of the inhibited systems, the R_{ct} is found to first rise steadily and reaches a maximum value; thereafter the R_{ct} is seen to attain a relatively stable state. It is believed that inhibition of metals corrosion by organic inhibitors is a substitution process whereby adsorbed water molecules are gradually replaced by inhibitor molecules [14]. NP-1-4-11-PUOPMOB molecules may have gradually substituted adsorbed water molecules on St37 steel surface and this resulted in the steady increase in R_{ct} with immersion time. The growth rate of the adsorbed NP-1-4-11-PUOPMOB layer may have reduced at a certain time resulting in the observed near constancy of charge transfer resistance. As could be seen from Fig. 6, the concentration of NP-1-4-11-PUOPMOB has direct effect on adsorption as well as the charge transfer resistance. For instance, R_{ct} vs t graphs for 25, 50, 100, 125, and 150 ppm inhibited acid solutions attain a steady state at 380, 410, 450, 820, and 1700 Ω cm^2 respectively.

The $R(QR)$ electrical equivalent circuit given in Fig. 7 was selected for the analysis of the DEIS data. The choice of this electrical equivalent circuit was necessitated by the small chi square value (did not exceed 3×10^{-4}) and fitting error (was < 20%) obtained for the analysis. In the equivalent circuit, R_s represents the uncompensated solution resistance, R_{ct} stands for the charge transfer resistance, and Q denotes the constant phase element (CPE) used in place of a double layer capacitor to account for the non-ideal behaviour of the St37 steel electrode [15]. The CPE can be modeled using the following equation [15]:

$$Z_{CPE} = [Q(j\omega)^n]^{-1} \quad (3)$$

where Z_{CPE} is the impedance, j the square root of -1, ω is the frequency, Q the capacitance, and n is a measure of non-homogeneity of the capacitor and takes a value in the range of $0 < n < 1$. All the electrochemical parameters derived from this process are given in Table 4. The percentage inhibition efficiency was computed from Eq. (4).

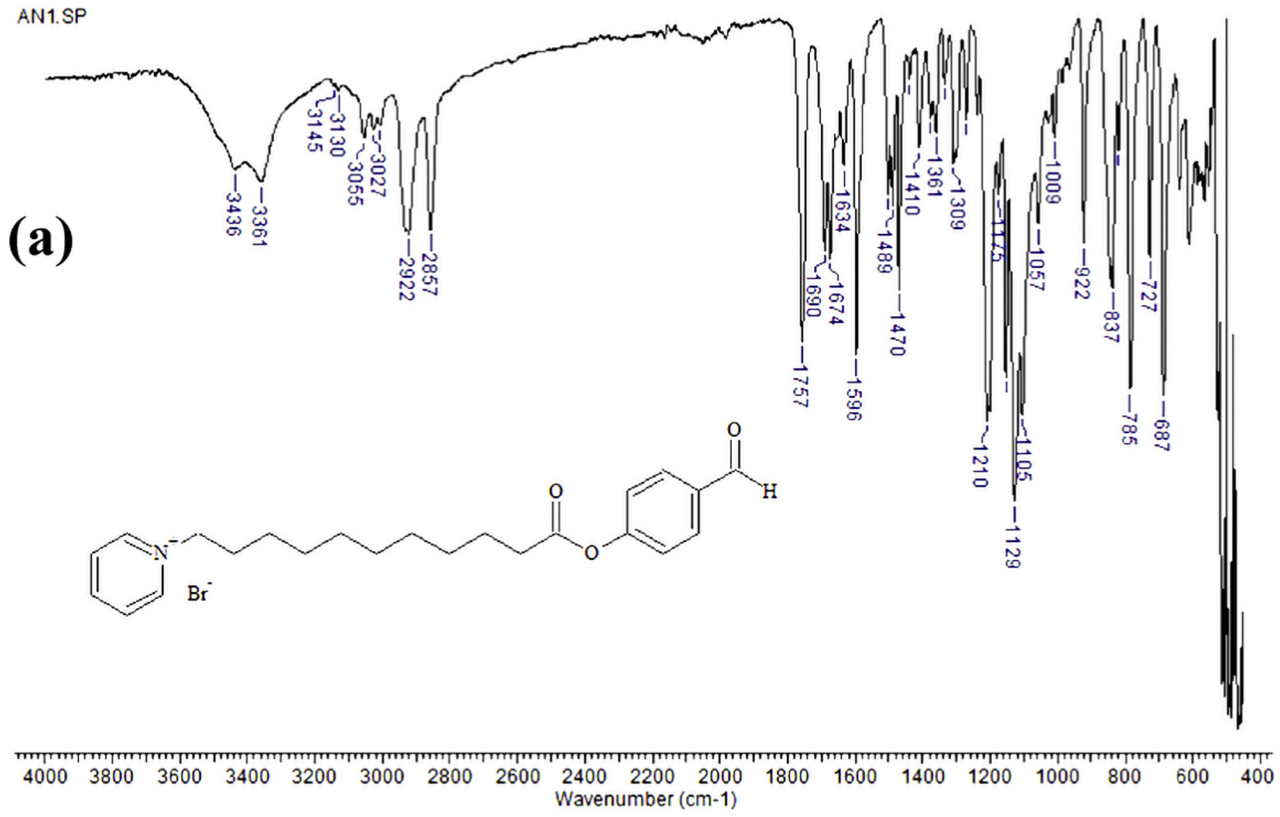

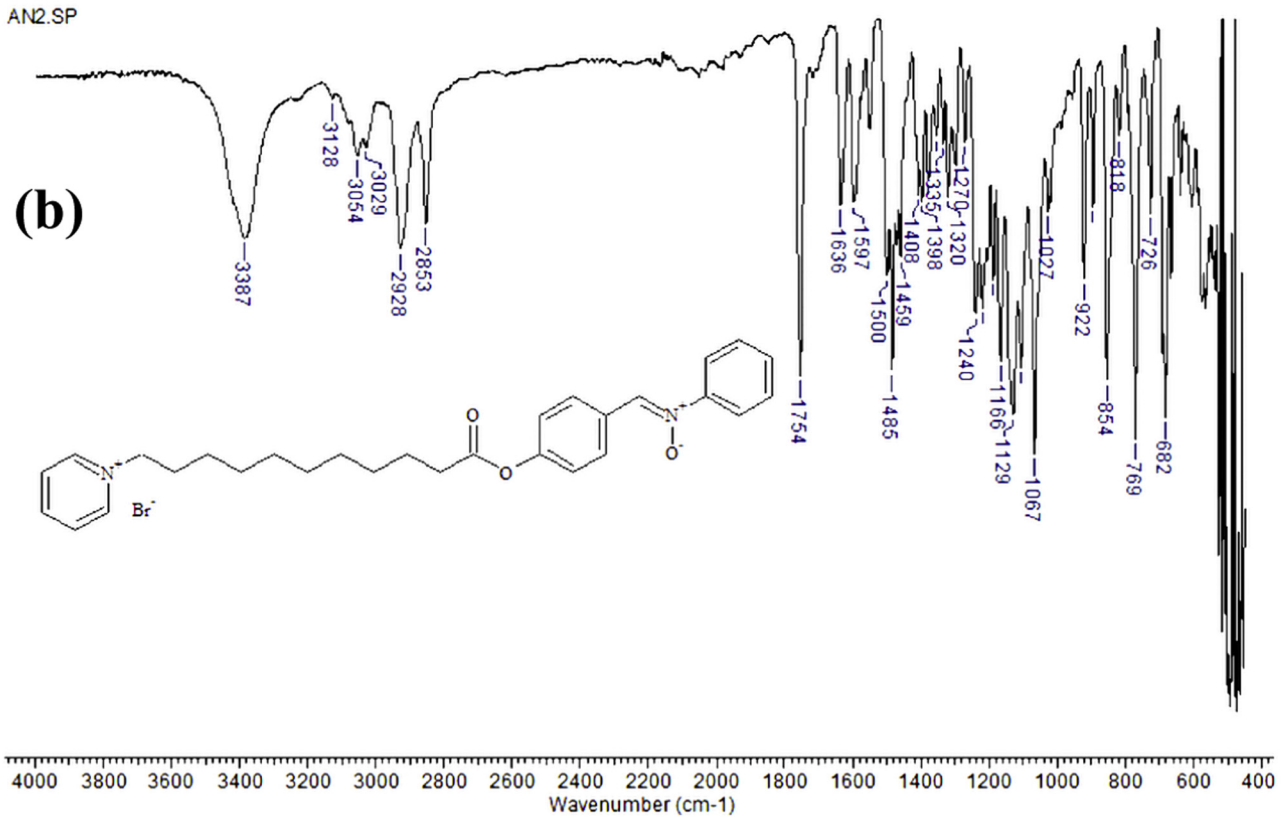

Fig. 4. FTIR spectrum of (a) amphiphilic nitrone **2** and (b) amphiphilic nitrone **3**.

Table 2
Spectral characterization data of compounds **2** and **3**.

Compound	Spectral data
2	**FT-IR, $\tilde{\nu}$/cm^{-1}**: 1757 (C=O stretch (ester)), 1690 (C=O stretch (aldehyde)), 1634 (C=N$^+$ stretch), 1129 (C–O stretch) **^{1}H NMR (600 MHz, DMSO-d_6)**: δ (ppm) = 9.98 (s, 1H, CHO), 9.12 (d, J = 5.4 Hz, 2H, Py), 8.59 (t, J = 7.8 Hz, 1H, Py), 8.15 (t, J = 7.2 Hz, 2H, Py), 7.96 (d, J = 8.4 Hz, 2H, Ar), 7.34 (d, J = 9 Hz, 2H, Ar), 4.60 (t, J = 7.8 Hz, 2H, N$^+$C$\underline{H_2}$CH$_2$), 2.59 (t, J = 7.8 Hz, 2H, −CH$_2$C$\underline{H_2}$COOAr), 1.89 (quin, J = 7.8 Hz, 2H, N$^+$CH$_2$C$\underline{H_2}$CH$_2$−), 1.61 (quin, J = 7.8 Hz, 2H, −CH$_2$C$\underline{H_2}$CH$_2$COOAr), 1.33 (quin, J = 7.8 Hz, 2H, N$^+$CH$_2$CH$_2$C$\underline{H_2}$CH$_2$−), 1.26–1.25 (m, 10H, −(CH$_2$)$_5$−). **^{13}C NMR (150 MHz, DMSO-d_6)**: δ (ppm) = 192.46, 171.82, 155.50, 145.91, 145.18, 134.27, 131.53, 128.52, 123.15, 61.16, 33.91, 31.15, 29.14, 29.06, 28.79, 28.77, 25.82, 24.64.
3	**FT-IR, $\tilde{\nu}$/cm^{-1}**: 1754 (C=O stretch (ester)), 1636 (C=N$^+$ stretch), 1551 (C=N stretch (nitrone)), 1067 (N$^+$–O$^-$ (nitrone)) **^{1}H NMR (600 MHz, DMSO-d_6)**: δ (ppm) = 9.11 (d, J = 6 Hz, 2H, Py), 8.59 (t, J = 7.8 Hz, 1H, Py), 8.53 (d, J = 6.6 Hz, 2H, Ar), 8.14 (t, J = 7.2 Hz, 2H, Py), 7.90 (d, J = 7.2 Hz, 2H, Ar), 7.55–7.49 (m, 3H, Ar), 7.24 (d, J = 9 Hz, 2H, Ar), 4.59 (t, J = 7.2 Hz, 2H, N$^+$C$\underline{H_2}$CH$_2$), 2.58 (t, J = 7.2 Hz, 2H, −CH$_2$C$\underline{H_2}$COOAr), 1.89 (quin, J = 7.2 Hz, 2H, N$^+$CH$_2$C$\underline{H_2}$CH$_2$−), 1.62 (quin, J = 7.8 Hz, 2H, −CH$_2$C$\underline{H_2}$CH$_2$COOAr), 1.34 (quin, J = 7.2 Hz, 2H, N$^+$CH$_2$CH$_2$C$\underline{H_2}$CH$_2$−), 1.26–1.25 (m, 10H, −(CH$_2$)$_5$−). **^{13}C NMR (150 MHz, DMSO-d_6)**: δ (ppm) = 172.03, 152.00, 148.82, 145.90, 145.17, 133.15, 130.62, 129.54, 129.22, 128.51, 122.31, 121.90, 61.18, 33.93, 31.15, 29.14, 29.06, 28.79, 25.83, 24.71.

Table 3
Weight loss (WL), corrosion rate (ν) and corrosion inhibition efficiency (η_{WL}) for varying concentrations of NP-1-4-11-PUOPMOB in 1 M HCl medium for 24 h at 25 °C.

Concentration (ppm)	WL (mg)	ν (mg cm^{-2} h^{-1})	η_{WL} (%)
0	4.07 ± 0.420	0.1696	–
25	0.89 ± 0.020	0.0371	78.13
50	0.70 ± 0.010	0.0291	82.80
100	0.54 ± 0.005	0.0225	86.73
125	0.33 ± 0.004	0.0138	91.74
150	0.21 ± 0.005	0.0088	94.84

$$\eta_{DEIS} = \left[1 - \frac{R_{ct}^{0}}{R_{ct}}\right] \times 100 \quad (4)$$

where R_{ct}^{0} is charge transfer resistance in the absence of NP-1-4-11-PUOPMOB and R_{ct} the charge transfer resistance in the presence of NP-1-4-11-PUOPMOB. From the results in Table 4, it is clear that the value of Q is smaller while that of R_{ct} is larger in the NP-1-4-11-PUOPMOB inhibited systems than in the uninhibited acid solution. By increasing the concentration of NP-1-4-11-PUOPMOB, Q value decreases while the reverse is observed for R_{ct} value. Consequently, the inhibition efficiency improved. For instance, the Q and R_{ct} values recorded in the blank solution are 342.5 μΩ^{-1} S^n cm^{-2} and 111.6 Ω cm^2 respectively. Addition of 25 ppm NP-1-4-11-PUOPMOB to the system decreases Q value to 306.2 μΩ^{-1} S^n cm^{-2} and increases R_{ct} value to 507.4 Ω cm^2. The corresponding inhibition efficiency is 78.0%. By increasing the concentration of NP-1-4-11-PUOPMOB to 50, 100, 125, and 150 ppm, Q value decreases to 233.5, 198.2, 131.4, and 80.2 μΩ^{-1} S^n cm^{-2} while R_{ct} value increases to 662.3, 751.2, 1146.3, and 1888.4 Ω cm^2 respectively. The η is stepped up from 78.0% to 83.1, 85.1, 90.3, and 94.1% respectively. A decrease in the local dielectric constant and/or an increase in the thickness of the electrical double layer could cause the value of Q to decrease. It is reasonable to assume that the observed decrease in Q value and increase in R_{ct} value with increasing NP-1-4-11-PUOPMOB concentration is due to an improved surface coverage leading to a more capacitive surface film. Also, worthy of note in Table 4 is the larger value of n in the inhibited acid solutions compared to the uninhibited and the fact that the value increases with increase in inhibitor concentration. As mentioned earlier, this parameter could be used as a gauge of surface heterogeneity. It could be said that the adsorption of NP-1-4-11-PUOPMOB molecules onto the steel surface increased the surface heterogeneity.

3.2.2.2. EIS studies. To further evaluate the protection ability of the synthesized NP-1-4-11-PUOPMOB, EIS measurements were performed. The representative Nyquist (a) and Bode modulus (b) plots of St37 steel immersed in 1 M HCl solution without and with NP-1-4-11-PUOPMOB are shown in Fig. 8. In Fig. 8(a), an individual capacitive loop appeared at high frequency, indicating that St37 steel corrosion in 1 M HCl solution is controlled by charge transfer at electrode/solution interface [17,19,48,49]. It is observed that the general shape of the Nyquist diagram is maintained in both inhibited and uninhibited systems. This suggests that the addition of NP-1-4-11-PUOPMOB does not alter the corrosion mechanism [16,49]. However, the addition of NP-1-4-11-PUOPMOB to the corrosive medium resulted in an increase in the diameter of the capacitive loop (Fig. 8(a)) and impedance modulus (Fig. 8(b)). Increase in NP-1-4-11-PUOPMOB concentration is found to cause further increase in both the diameter of the capacitive loop and the impedance modulus. This suggests larger surface coverage and corrosion protection with the increasing of NP-1-4-11-PUOPMOB concentration. Also worthy of note in Fig. 8(a) is the imperfectness of the capacitive loop at high frequency. This is typical of a charge controlled corrosion process [14,18].

The Nyquist data were analyzed using the same $R(QR)$ electrical equivalent circuit (Fig. 7) selected for the analysis of the DEIS data and the derived electrochemical parameters are also listed in Table 4. The Q, R_{ct}, and n parameters vary in similar manner as those derived and discussed under DEIS studies. The η values obtained from this method compares well with those from the DEIS technique. The η value of 94.4% is afforded by the highest studied concentration (150 ppm).

3.2.2.3. PDP studies. Fig. 9 illustrates the potentiodynamic polarization curves of St37 steel in 1 M HCl solution devoid of and containing different concentrations of NP-1-4-11-PUOPMOB at 25 °C. The polarization curves composed of two branches representing the anodic Fe oxidation and cathodic hydrogen ions reduction reactions. A comparison of the polarization curve recorded in the free acid solution to those in the NP-1-4-11-PUOPMOB inhibited acid solutions discloses that the anodic and cathodic current densities are shifted to lower values in the inhibited curves and the corrosion potential slightly displaced anodically. This effect is found to be a function of inhibitor concentration; that is, the highest studied concentration produced the greatest effect. This demonstrates the inhibiting power of NP-1-4-11-PUOPMOB which is augmented with increasing inhibitor concentration. The slight displacement of the corrosion potential toward the anodic direction suggest that NP-1-4-11-PUOPMOB behaves in 1 M HCl solution as a mixed type corrosion inhibitor but with greater effect on the anodic processes.

The polarization parameters such as corrosion potential (E_{corr}), corrosion current (I_{corr}), as well as the anodic and cathodic Tafel slopes (β_a and β_c) derived from the potentiodynamic curves via extrapolation technique are presented in Table 5. Inhibition efficiency was computed from the I_{corr} values according to the following equation:

$$\eta_{PDP}(\%) = \left[1 - \frac{I_{corr}}{I_{corr}^{0}}\right] \times 100 \quad (5)$$

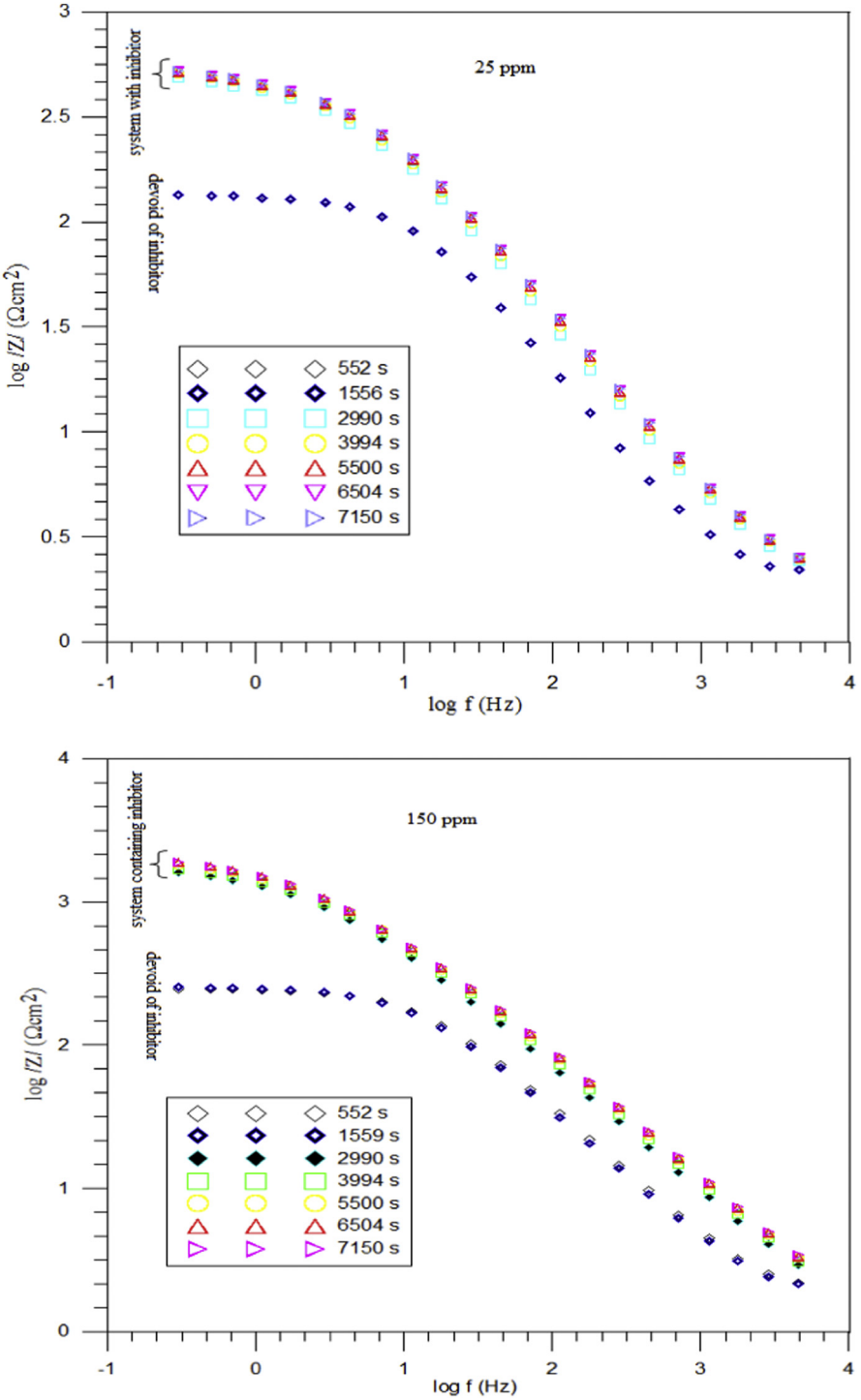

Fig. 5. DEIS spectra for St37 steel in 1 M HCl containing 25 ppm and 150 ppm NP-1-4-11-PUOPMOB respectively at different measurement times in Bode modulus representation.

where $I_{corr}{}^{0}$ is the corrosion current density in the absence of NP-1-4-11-PUOPMOB and I_{corr}, is the corrosion current density in the presence of NP-1-4-11-PUOPMOB. As is expected, the I_{corr} of the inhibited systems are smaller compared to that of the uninhibited and further decreases with increasing inhibitor concentration. For instance, the addition of 25 ppm NP-1-4-11-PUOPMOB to the acid solution decrease I_{corr} from 120 μA cm^{-2} to 24 μA cm^{-2} and this corresponds to η of 77.5%. By increasing the concentration of the inhibitor to 150 ppm, I_{corr} declines significantly to 6 μA cm^{-2} and the η also greatly improves to 94.2%. This again supports the claim from EIS studies that the decrease in the value of Q and increase in R_{ct} value with increasing inhibitor concentration was due to an improved surface coverage leading to an effective surface protection. It also shows that the 150 ppm NP-1-4-11-PUOPMOB is capable of providing an appreciable protection to steel surface in 1 M HCl solution.

A further inspection of Table 5 reveals that β_a value increase with increasing inhibitor concentration whereas β_c value shows no pattern with concentration. The non-pattern of β_c value with increasing inhibitor concentration suggests non-alteration of the mechanism of cathodic reactions [23]. The increase in β_a value with increasing NP-1-

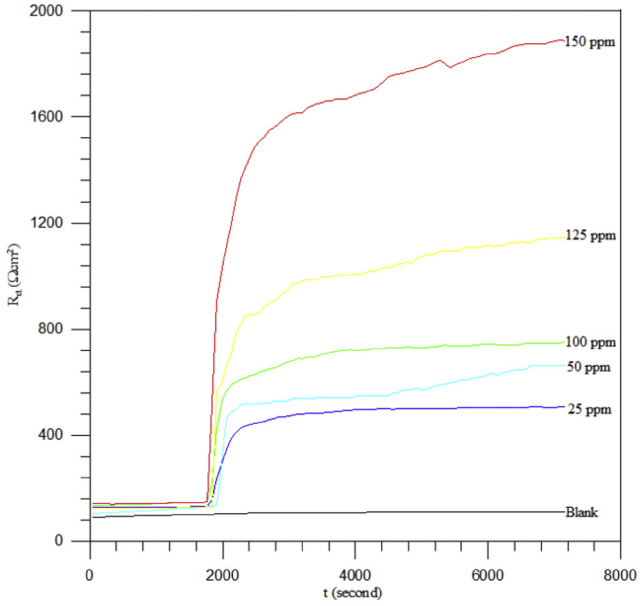

Fig. 6. Plot of R_{ct} as a function of immersion time (s) for St37 steel in 1 M HCl in the absence and presence of different concentrations of NP-1-4-11-PUOPMOB.

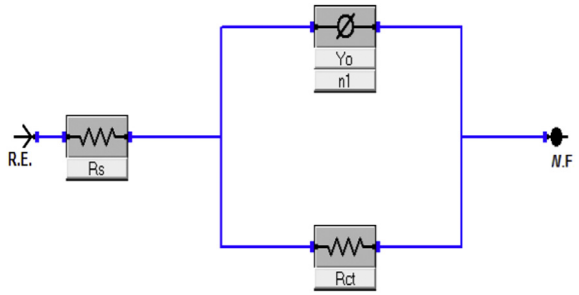

Fig. 7. Equivalent circuit model used to fit Nyquist experimental data.

Table 4
Dynamic electrochemical impedance parameters for St37 steel in 1 M HCl in the absence and presence of various concentrations of NP-1-4-11-PUOPMOB at 25 °C.

Concentration (ppm)	R_s (Ω cm^2)	Q		R_{ct} (Ω cm^2)	η (%)
		Y_0 ($\mu\Omega^{-1}$ S^n cm^{-2})	n ($0 \le n \le 1$)		
DEIS					
0	2.02	342.5	0.78	111.6	–
25	2.04	306.2	0.81	507.4	78.0
50	2.03	233.5	0.84	662.3	83.1
100	2.06	198.2	0.88	751.2	85.1
125	1.96	131.4	0.89	1146.3	90.3
150	1.54	80.2	0.92	1888.4	94.1
EIS					
0	1.90	336.5	0.79	109.4	–
25	2.19	311.2	0.84	472.3	76.8
50	1.95	240.7	0.89	638.4	82.9
100	1.90	186.6	0.92	764.5	85.7
125	1.79	127.3	0.93	1139.2	90.4
150	1.59	83.8	0.94	1958.4	94.4

4-11-PUOPMOB concentration may suggest modification of the mechanism of anodic reactions by adsorbed NP-1-4-11-PUOPMOB molecules [16]. It is pertinent to mention here that the values of η obtained from all the applied techniques in this study are in perfect agreement with each other and compare very well with the values obtained by other researchers for organic inhibitor containing pyridinium moiety (Table 1).

3.3. Adsorption studies

Adsorption is an important factor that defines the performance of an organic inhibitor on corrosion of metals. A study of adsorption isotherm can provide insight into the kind of interaction between NP-1-4-11-PUOPMOB molecules and St37 steel surface in 1 M HCl solution. For this purpose, surface coverage (θ) value was computed from the values of η ($\theta = \eta/100$) obtained from weight loss measurements. The θ values were fitted into different adsorption isotherms in order to find the best fit. The value of linear regression (R^2) was used as a gauge. A value of $R^2 = 1$ defines a perfect fit. In our case, the best fit was obtained for Langmuir adsorption isotherm (Fig. 10) which has the form [50–52]

$$\frac{C_{inh}}{\theta} = \frac{1}{K_{ads}} + C_{inh} \quad (6)$$

where C_{inh} is the concentration of inhibitor in mM, θ is the surface coverage, and K_{ads} is the equilibrium constant of adsorption-desorption process in L g^{-1}. The slope of Fig. 10 slightly deviated from unity required by an ideal Langmuir isotherm plot. Interaction in the adsorbed layer might be the reason [5,50–54]. The K_{ads} value computed from the intercept of the linear graphs in Fig. 10 is 58.82×10^3 L g^{-1}. As mentioned earlier, K_{ads} value denotes the strength of the bond between adsorbed inhibitor molecules and the metal surface. As could be seen from Fig.1, the investigated inhibitor is characterized by a pyridinium ring structure with delocalized π electrons (aromaticity). These structural feature favors the interaction of the inhibitor with St37 steel surface. Additionally, the presence of N, O atoms and conjugated double bonds in the structure of nitrone makes the formation of p–d bonds resulting from overlap of p-electrons to the 3d vacant orbital of iron atoms possible and this enhances the adsorption of the inhibitor on the steel surface [55,56]. The higher magnitude of K_{ads} reflect the strong adsorption bond between NP-1-4-11-PUOPMOB molecules and St37 steel surface. The K_{ads} value was used to calculate the free energy of adsorption (ΔG_{ads}^0) as follows:

$$\Delta G_{ads}^0 = -RT \ln(55.5 \times K_{ads}) \quad (7)$$

where R is the universal gas constant, T is the absolute temperature and 55.5 is the molar concentration of water in mol dm^{-3} in the solution. The calculated ΔG_{ads}^0 value is -37.16 kJ mol^{-1} pointing to the spontaneity of the process.

3.4. Surface analysis

Fig. 11 presents the SEM images for St37 steel immersed in 1 M HCl solution (a) without and (b) with 150 ppm NP-1-4-11-PUOPMOB for 24 h at 25 °C. The elemental composition (wt%) of the corrosion products and/or protective film deposited on the surfaces in Fig. 11 obtained from EDAX analysis is summarized in Table 6. Clearly, deposits of corrosion products can be seen on the surface in Fig. 11(a). The high percentage weight of O (19.00%) and Cl (15.66%) in Table 6 suggests that the observed deposits are composed of oxides and chlorides of Fe. Ji et al. [57] recently established through the use of X-ray photoelectron spectroscopy to examine the surface of Q235 steel exposed to 1 M HCl solution that the corrosion products were mostly Fe_2O_3, $FeCl_3$, FeOH and/or $Fe(OH)_3$. Corrosion products can interrupt corrosion processes on a metal surface but cannot offer long term protection as they are unstable. Fig. 11(a) confirms this assertion. It appears from Fig. 11(a), that the surface is seriously damaged and is characterized with pits and cavities. By comparing the surface in Fig. 11(a) to that in Fig. 11(b), one could see that the surface in Fig. 11(b) are covered with a more compact film. It could be said, based on the EDAX results in Table 6 that the film in Fig. 11(b) is formed by adsorbed NP-1-4-11-PUOPMOB molecules (N, 0.87% and Br, 0.67% are component

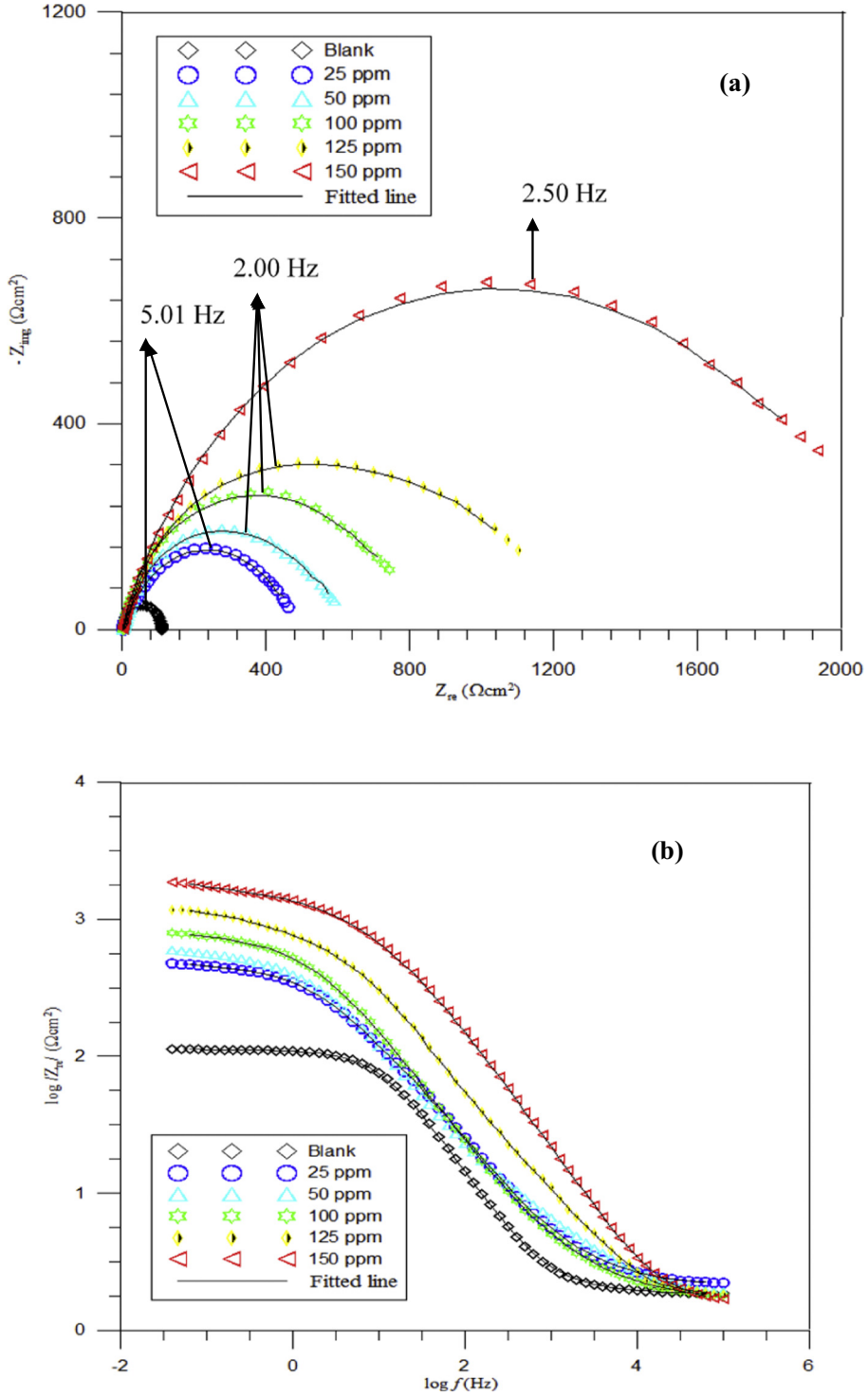

Fig. 8. Electrochemical impedance spectra for St37 steel in 1 M HCl solution in the absence and presence of various concentrations of NP-1-4-11-PUOPMOB in (a) Nyquist and (b) Bode modulus representations.

elements of NP-1-4-11-PUOPMOB). This film protects the specimen surfaces against corrosion.

AFM is a powerful technique to investigate the surface morphology at nano- to microscale and has become a new choice to study the inhibitive effect of inhibitors against to the corrosion at the metal/solution interface. AFM gives important information about surface properties, surface morphology, surface roughness and surface elasticity [58]. The three dimensional AFM images of the steel surface exposed to 1 M HCl with and without 150 ppm of inhibitor solution for 24 h are shown in Fig. 12. Fig. 12(a) shows the metal surface exposed to 1.0 M HCl in the absence of the inhibitor. As shown in Fig. 12(a), a rough structure with large and wide cavities was formed on the metal surface. The roughness average of the surface was 415.77 nm. On the other hand, Fig. 12(b) shows the metal surface exposed to 1.0 M HCl with the addition of 150 ppm of inhibitor for 24 h. With the adsorption of the inhibitor molecules to the metal surface, a smoother and more uniform surface was observed when compared to the surface treated with uninhibited 1 M HCl solution. The size and width of the cavities on the

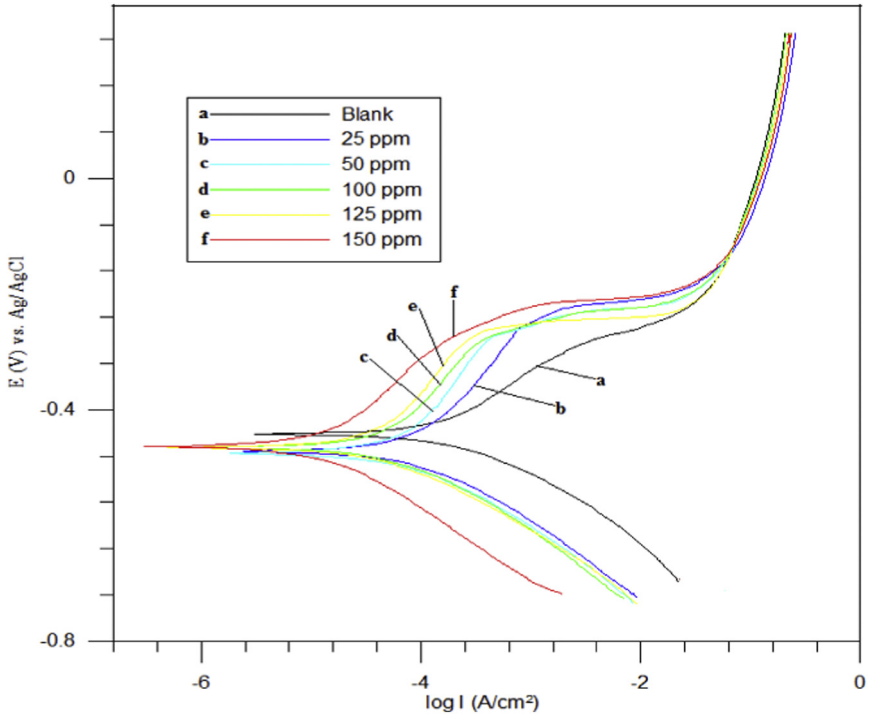

Fig. 9. Potentiodynamic polarization curves obtained for St37 steel in 1 M HCl solution devoid and containing various concentrations of NP-1-4-11-PUOPMOB at 25 °C.

Table 5
Potentiodynamic polarization parameters for St37 steel in 1 M HCl in the absence and presence of various concentrations of NP-1-4-11-PUOPMOB at 25 °C.

Concentration (ppm)	β_a (mV dec^{-1})	$-\beta_c$ (mV dec^{-1})	$-E_{corr}$ ($mV_{Ag/AgCl}$)	I_{corr} (μA cm^{-2})	η_{PDP} (%)
0	114	88	441	120	–
25	239	115	472	27	77.5
50	257	112	475	21	83.0
100	275	110	465	16	86.7
125	278	111	467	12	90.0
150	285	109	464	7	94.2

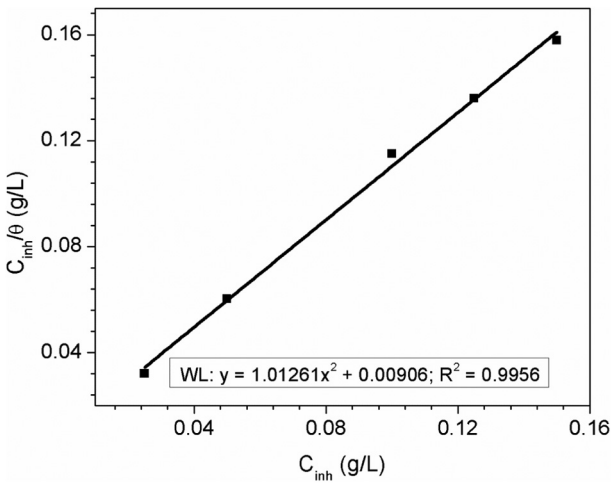

Fig. 10. Langmuir plot of $C_{inh}\backslash\theta$ versus C_{inh} for St37 steel in 1 M HCl solution containing NP-1-4-11-PUOPMOB.

surface was definitely decreased and the roughness average of the surface was 54.79 nm.

3.5. Quantum chemical studies

It is worth emphasizing that a DFT-based approach allows accurate calculations of a number of physical and chemical properties of several compounds as corrosion inhibitors, some of which can either be compared directly to experiment or are complementary to it [59]. As is well-known, adsorption of an inhibitor on a metal surface means that the inhibitor-adsorbed area is resistant to corrosion. Inhibitor molecules can absorb onto the surface in different ways, and when it comes to physisorption, physisorbed molecules are trapped in a shallow potential energy well and usually remain mobile in the plane of the surface. On the other hand, chemisorption comes to the forefront when a chemical bond is formed between the inhibitor and surface. Unlike physisorption, chemisorbed products are mostly immobile (except H-atoms) on the surface and bind to specific surface sites [60]. The chemical bond between inhibitor and the surface can be considered a combination of doubly interactions of the highest occupied molecular orbitals (HOMO) and the lowest unoccupied molecular orbitals (LUMO). It is apparent from the molecular orbital distributions depicted in Fig. 13, that the HOMO is almost exclusively centered on the N and O atoms of nitrosobenzene fragment, whereas the LUMO is mainly the p-bonding orbital between the C and N atoms of pyridinyl group. NP-1-4-11-PUOPMOB molecule has asymmetric charge distributions that result in molecular dipole moment of ~56 D in both phases (Table 7). This permanent dipole moment is the result mostly of the asymmetric distribution of negative charges, which are found at the O, N and some C atoms of nitrosobenzene fragment. A dipole of this magnitude is expected to enhance considerably the inhibition efficiency of the compound [59]. In Table 7; the eigen values (energies) of the HOMOs and LUMOs are also listed, as well as the energy gap (ΔE), the difference between HOMO and LUMO. This gap is a measure of electron conductivity and indicates the capability of electronic transitions from occupied orbitals to unoccupied ones. Based within Hartree–Fock

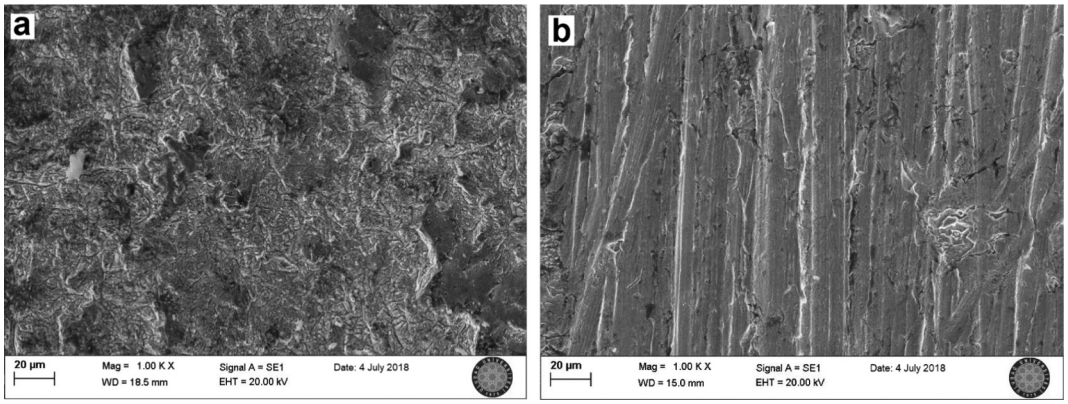

Fig. 11. SEM images for St37 steel in 1 M HCl solution (a) without NP-1-4-11-PUOPMOB and (b) containing 150 ppm NP-1-4-11-PUOPMOB after 24 h of exposure at 25 °C.

Table 6
Elemental composition (wt%) of the corrosion products/protective film on the St37 steel surface immersed in 1 M HCl solution without and with 150 ppm NP-1-4-11-PUOPMOB from EDAX analysis.

Element	Specimen surface exposed to 1 M HCl solution	Specimen surface exposed to 1 M HCl solution containing 150 ppm NP-1-4-11-PUOPMOB
C	0.83	3.06
O	19.00	16.42
Mg	0.04	0.29
Si	0.14	0.37
Cl	15.66	5.86
Fe	64.33	72.44
N	–	0.87
Br	–	0.67
Total (%)	100.00	100.00

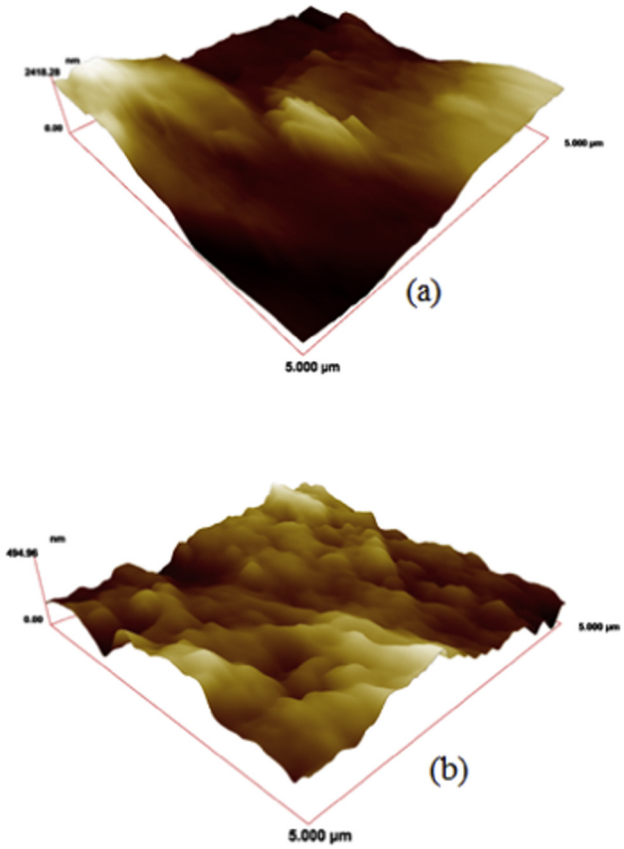

Fig. 12. AFM images for St37 steel after exposure to (a) 1 M HCl solution, and (b) 1 M HCl solution containing 150 ppm NP-1-4-11-PUOPMOB for 24 h at 25 °C.

theory, Koopmans' theorem [61] (i.e., frozen orbital approximation) states that the ionization potential (I) of the neutral ground state is given by the sign inverse of the HOMO energy and that the electron affinity (A) is given by the LUMO energy. The chemical hardness (φ) and electronegativity (χ) are defined as $\varphi = (-E_{HOMO} + E_{LUMO})/2$ and $\chi = (-E_{HOMO} - E_{LUMO})/2$, and the fraction of electrons transferred (ΔN) is calculated by $\Delta N = (\chi_{Fe} - \chi_{inh})/2(\varphi_{Fe} - \varphi_{inh})$, where experimental polycrystalline work function value of bulk iron, $\chi_{Fe} = 4.5$ eV [62], and a global hardness of $\varphi_{Fe} = 0$ eV were used based on the assumption that for a bulk metal $I = A$ because they are softer than the neutral metallic atoms. If $\Delta N < 3.6$, the inhibition efficiency enhances with increasing electron-donating ability to the metal surface, and due to higher electronegativity of NP-1-4-11-PUOPMOB compared to the densely packed steel surface, the charge would flow to inhibitor from metal surface as evidenced in the study of Lukovits et al. [63].

3.6. Corrosion inhibition mechanism

The inhibition efficiency of the inhibitor material generally depends on various factors, such as the number of adsorption sites, charge density, molecular size, and mode of interaction with the metal surface to form a metallic complex. The electron-donor N-oxide oxygen atom of a nitrone makes it suitable for complexation and protonation. The nitrone molecules tend to be adsorbed on to the mild steel substrate as a negatively charged species which can form a complex with the positive metal cation Fe^{2+} [33]. The corrosion inhibition of the synthesized amphiphilic nitrone in 1.0 M HCl may be due to the adsorption of this compound on the metal surface by the following interactions [64]. (1) Interaction between p-electrons of the two benzenes and pyridinium rings with the positively charged metal surface; (2) Interaction between lone pairs of electrons of oxygen atoms with the positively charged metal surface. These possible interactions between the synthesized nitrone and metal surface are given in Fig. 14.

It is known that halide ions increase the inhibiting tendency of the positive quaternary ammonium ion by synergistic effect [65–67]. The bromide ion of the nitrone compound and the chloride ion of HCl may adsorb on the metal surface. The bromide ion is more apt to adsorption compared to chloride ion because the electronegativity of chloride anion is higher than that of bromide (Br^- = 2.8, Cl^- = 3.0), and the atomic radius of bromide anion is larger than chloride anion (Br^- = 114 pm, Cl^- = 90 pm) [66]. The halide ion adsorbs on the positively charged metal surface via chemisorption to create dipoles in acidic solutions and these dipoles change the charge of the metal surface from positive to negative. After this strong chemical adsorption of

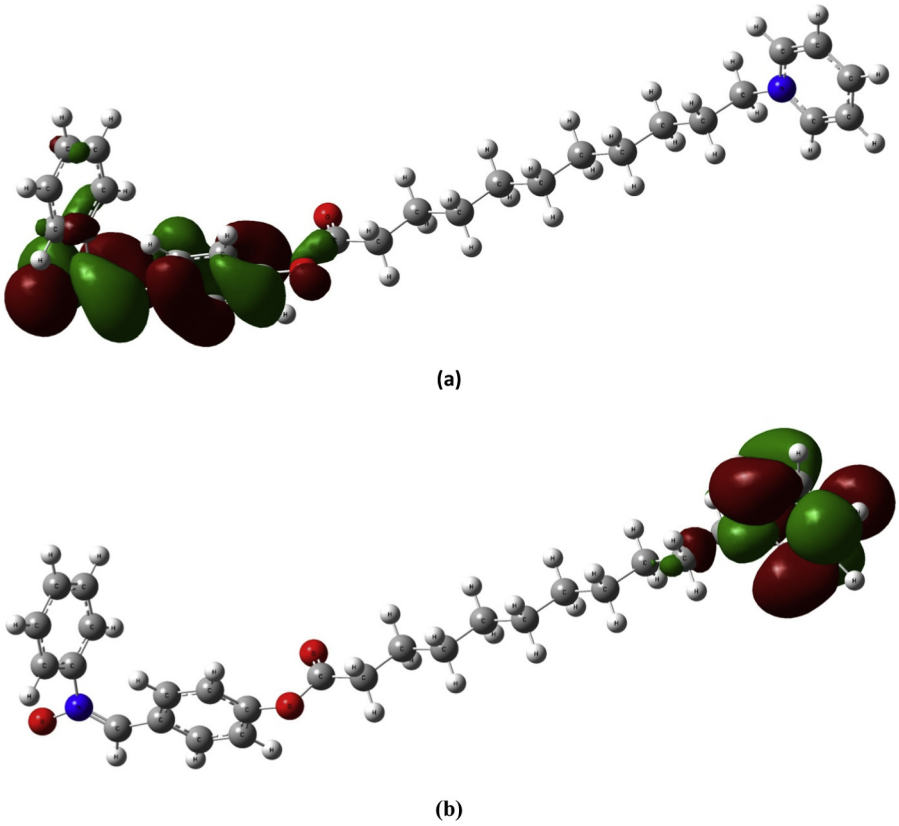

Fig. 13. Molecular orbital surfaces for (a) HOMO and (b) LUMO of NP-1-4-11-PUOPMOB.

Table 7
The calculated quantum chemical parameters at the B3LYP/6-311G + +(d,p) basis set for NP-1-4-11-PUOPMOB in gas and aqueous phases.

Phase[a]	E_{HOMO} (eV)	E_{LUMO} (eV)	ΔE ($E_L - E_H$) (eV)	μ (D)	χ	φ	ΔN
G	−6.631	−5.738	0.893	56.363	6.185	0.447	−1.884
A	−6.201	−2.755	3.446	54.751	4.478	1.723	0.001

[a] G – gas phase (ε = 1.0), A – aqueous phase (ε = 78.5).

halide ions, the cationic pyridinium group of the molecule is then adsorbed on the negatively charged metal surface by electrostatic attraction. This cooperation between the adsorbed halide ions with cationic group of the inhibitors lead to a greater surface coverage and thus greater inhibition [28,66]. Along with that, the electron-donor N-oxide oxygen atom of the nitrone can be protonated in acidic medium. Gu et al. [18] by using X-ray photoelectron spectroscopy studied the adsorption and corrosion inhibition of X70 steel in 1 M HCl solution by N-alkyl-2-(4-hydroxybut-2-ynyl) pyridinium bromide, and they found that

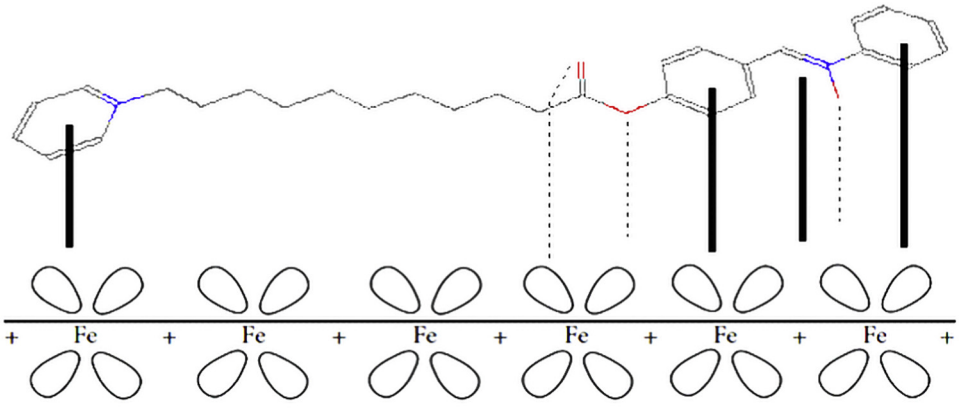

Fig. 14. The adsorption of synthesized nitrone compound on the steel surface by coordination.

the halide ions can adsorb sufficiently on steel surface and effectively replenish the surface such that strong attractive interaction between the surface and charged inhibitor species is afforded. This may have been the case with NP-1-4-11-PUOPMOB as suggested by high K_{ads} value. Again, diaryl nitrones unlike alkyl nitrones are generally resistant to hydrolysis, and therefore, it is considered that the possible hydrolysis products, phenylhydroxylamine and related carbonyl compound, are not effective during corrosion inhibition [68].

4. Conclusion

A new amphiphilic nitrone (NP-1-4-11-PUOPMOB) with superior corrosion inhibition efficiency has been synthesized and characterized by FT-IR, ^{1}H and ^{13}C NMR. The corrosion inhibitive power of NP-1-4-11-PUOPMOB on St37 steel in 1 M HCl has been assessed using both experimental and theoretical approaches. Results from EIS and DEIS show that the presence of the nitrone in the corrosive medium causes an increase in the charge transfer resistance of the metal specimen. The inhibitive effect of the inhibitor varies directly with concentration. Results from polarization studies reveal that NP-1-4-11-PUOPMOB suppressed both the cathodic and anodic corrosion processes i.e., the inhibitor behaved as a mixed type corrosion inhibitor. Inhibition is via an adsorption mechanism which is best described using Langmuir adsorption isotherm. The K_{ads} values show strong interaction between NP-1-4-11-PUOPMOB molecules and St37 steel surface. There is evidence of NP-1-4-11-PUOPMOB adsorption on the metal surface from SEM, EDAX, and AFM studies. Experimental and theoretical results are in good agreement.

References

[1] P. Altoe, G. Pimenta, C.F. Moulin, S.L. Diaz, O.R. Mattos, Evaluation of oilfield corrosion inhibitors in CO_2 containing media: a kinetic study, Electrochim. Acta 41 (1996) 1165–1172.

[2] D. Dwivedi, K. Lepková, T. Becker, Carbon steel corrosion: a review of key surface properties and characterization methods, RSC Adv. 7 (2017) 4580–4610.

[3] A. Yıldırım, M. Çetin, Synthesis and evaluation of new long alkyl side chain acetamide, isoxazolidine and isoxazoline derivatives as corrosion inhibitors, Corros. Sci. 50 (2008) 155–165.

[4] S. Pathan, S. Ahmad, S-triazine ring-modified waterborne alkyd: synthesis, characterization, antibacterial, and electrochemical corrosion studies, ACS Sustain. Chem. Eng. 1 (2013) 1246–1257.

[5] Y. Ma, F. Han, Z. Li, C. Xia, Acidic-functionalized ionic liquid as corrosion inhibitor for 304 stainless steel in aqueous sulfuric acid, ACS Sustain. Chem. Eng. 4 (2016) 5046–5052.

[6] A. Dandia, S.L. Gupta, P. Singh, M.A. Quraishi, Ultrasound-assisted synthesis of pyrazolo[3,4 b] pyridines as potential corrosion inhibitors for mild steel in 1.0 M HCl, ACS Sustain. Chem. Eng. 1 (2013) 1303–1310.

[7] M. Yadav, R.R. Sinha, T.K. Sarkar, I. Bahadur, E.E. Ebenso, Application of new isonicotinamides as a corrosion inhibitor on mild steel in acidic medium: electrochemical, SEM, EDX, AFM and DFT investigations, J. Mol. Liq. 212 (2015) 686–698.

[8] C. Verma, E.E. Ebenso, I. Bahadur, I.B. Obot, M.A. Quraishi, 5-(Phenylthio)-3H-pyrrole-4-carbonitriles as effective corrosion inhibitors for mild steel in 1 M HCl: experimental and theoretical investigation, J. Mol. Liq. 212 (2015) 209–218.

[9] N. Yilmaz, A. Fitoz, Ü. Ergun, K.C. Emregül, A combined electrochemical and theoretical study into the effect of 2-((thiazole-2-ylimino)methyl)phenol as a corrosion inhibitor for mild steel in a highly acidic environment, Corros. Sci. 111 (2016) 110–120.

[10] Z. Hu, Y. Meng, X. Ma, H. Zhu, J. Li, C. Li, D. Cao, Experimental and theoretical studies of benzothiazole derivatives as corrosion inhibitors for carbon steel in 1 M HCl, Corros. Sci. 112 (2016) 563–575.

[11] M. Yadav, S. Kumar, R.R. Sinha, I. Bahadur, E.E. Ebenso, New pyrimidine derivatives as efficient organic inhibitors on mild steel corrosion in acidic medium: electrochemical, SEM, EDX, AFM and DFT studies, J. Mol. Liq. 211 (2015) 135–145.

[12] J. Wysocka, S. Krakowiak, J. Ryl, K. Darowicki, Investigation of the electrochemical behaviour of AA1050 aluminium alloy in aqueous alkaline solutions using dynamic electrochemical impedance spectroscopy, J. Electroanal. Chem. 778 (2016) 126–136.

[13] M.M. Solomon, H. Gerengi, T. Kaya, E. Kaya, S.A. Umoren, Synergistic inhibition of St37 steel corrosion in 15% H_2SO_4 solution by chitosan and iodide ion additives, Cellulose 24 (2017) 931–950.

[14] M.M. Solomon, H. Gerengi, T. Kaya, S.A. Umoren, Performance evaluation of a chitosan/silver nanoparticles composite on St37 steel corrosion in a 15% HCl solution, ACS Sustain. Chem. Eng. 5 (2017) 809–820.

[15] H. Gerengi, G. Bereket, M. Kurtay, Morphological and electrochemical comparison of the corrosion process of aluminum alloys under simulated acid rain conditions, J. Taiwan Inst. Chem. Eng. 58 (2016) 509–516.

[16] H. Gerengi, M. Mielniczek, G. Gece, M.M. Solomon, Experimental and quantum chemical evaluation of 8-hydroxyquinoline as a corrosion inhibitor for copper in 0.1 M HCl, Ind. Eng. Chem. Res. 55 (2016) 9614–9624.

[17] L. Wang, G.J. Yin, J.G. Yin, 2-Mercaptothiazoline and cetyl pyridinium chloride as inhibitors for the corrosion of a low carbon steel in phosphoric acid, Corros. Sci. 43 (2001) 1197–1202.

[18] T. Gu, Z. Chen, X. Jiang, L. Zhou, Y. Liao, M. Duan, H. Wang, Q. Pu, Synthesis and inhibition of N-alkyl-2-(4-hydroxybut-2-ynyl) pyridinium bromide for mild steel in acid solution: Box–Behnken design optimization and mechanism probe, Corros. Sci. 90 (2015) 118–132.

[19] Q. Yu, X. Jiang, L. Zhou, Y. Liao, M. Duan, H. Wang, Q. Pu, Synthesis and anticorrosion for X70 steel of propynol derivatives in acid medium, J. Mater. Environ. Sci. 5 (2014) 13–32.

[20] N.V. Likhanova, M.A. Dominguez-Aguilar, Q. Olivares-Xomet, N. Nava-Entzana, E. Arce, H. Dorantes, The effect of ionic liquids with imidazolium and pyridinium cations on the corrosion inhibition of mild steel in acidic environment, Corros. Sci. 52 (2010) 2088–2097.

[21] S. Tu, X. Jiang, L. Zhou, M. Duan, H. Wang, X. Jiang, Synthesis of N-alkyl-4-(4-hydroxybut-2-ynyl) pyridinium bromides and their corrosion inhibition activities on X70 steel in 5 M HCl, Corros. Sci. 65 (2012) 13–25.

[22] G. Xia, X. Jiang, L. Zhou, Y. Liao, M. Duan, H. Wang, Q. Pu, J. Zhou, Synergic effect of methyl acrylate and N-cetyl pyridinium bromide in N-cetyl-3-(2-methoxycarbonylvinyl)pyridinium bromide molecule for X70 steel protection, Corros. Sci. 94 (2015) 224–236.

[23] G. Xia, X. Jiang, L. Zhou, Y. Liao, M. Duan, H. Wang, Q. Pu, J. Zhou, Enhanced anticorrosion of methyl acrylate by covalent bonded N-alkyl pyridinium bromide for X70 steel in 5 M HCl, J. Ind. Eng. Chem. 27 (2015) 133–148.

[24] S.A. Abd El-Maksoud, The effect of hexadecyl pyridinium bromide and hexadecyl trimethyl ammonium bromide on the behaviour of iron and copper in acidic solutions, J. Electroanal. Chem. 565 (2004) 321–328.

[25] M.M. Saleh, Inhibition of mild steel corrosion by hexadecyl pyridinium bromide in 0.5 M H_2SO_4, Mater. Chem. Phys. 98 (2006) 83–89.

[26] M.M. Hamza, S.S. Abd El Rehim, M.A.M. Ibrahim, Inhibition effect of hexadecyl pyridinium bromide on the corrosion behavior of some austenitic stainless steels in H_2SO_4 solutions, Arab. J. Chem. 6 (2013) 413–422.

[27] E.A. Noor, A.H. Al-Moubaraki, Thermodynamic study of metal corrosion and inhibitor adsorption processes in mild steel/1-methyl-4[4-(-X)-styryl] pyridiniumiodides/hydrochloric acid systems, Mater. Chem. Phys. 110 (2008) 145–154.

[28] S. Öztürk, A. Yıldırım, M. Çetin, M. Tavaslı, Synthesis of quaternary, long-chain N-alkyl amides and their corrosion inhibition in acidic media, J. Surfactant Deterg. 17 (2014) 471–481.

[29] A. Yıldırım, S. Öztürk, M. Çetin, Novel amide-based cationic surfactants as efficient corrosion inhibitors for carbon steel in HCl and H_2SO_4 media, J. Surfactant Deterg. 16 (2013) 13–23.

[30] M.A. Hegazy, S.S. Abd El-Rehim, E.A. Badr, W.M. Kamel, A.H. Youssif, Mono-, di- and tetra-cationic surfactants as carbon steel corrosion inhibitors, J. Surfactant Deterg. 18 (2015) 1033–1042.

[31] D. Asefi, M. Arami, N.M. Mahmoodi, Electrochemical effect of cationic gemini surfactant and halide salts on corrosion inhibition of low carbon steel in acid medium, Corros. Sci. 52 (2010) 794–800.

[32] A.S. Fouda, Y.A. Elewady, H.K. Abd El-Aziz, A.M. Ahmed, Corrosion inhibition of carbon steel in 0.5 M HCl solution using cationic surfactants, Int. J. Electrochem. Sci. 7 (2012) 10456–10475.

[33] M. Thirumalaikumar, S. Jegannathan, Inhibition effects of nitrones on the corrosion of mild steel in organic acid media, Port. Electrochim. Acta 29 (2011) 1–8.

[34] S. Chen, K. Zhao, G. Chen, Synthesis and application of phenyl nitrone derivatives as acidic and microbial corrosion inhibitors, J. Chem. 2015 (2015) 1–6.

[35] S.U. Rahman, M.T. Saeed, S.A. Ali, Cyclic nitrones as novel organic corrosion inhibitors for carbon steel in acidic media, Anti Corros. Method M. 52 (2005) 154–159.

[36] G. Durand, R.A. Prosak, Y. Han, S. Ortial, A. Rockenbauer, B. Pucci, F.A. Villamena, Spin trapping and cytoprotective properties of fluorinated amphiphilic carrier conjugates of cyclic versus linear nitrones, Chem. Res. Toxicol. 22 (9) (2009) 1570–1581.

[37] G. Durand, B. Poeggeler, S. Ortial, A. Polidori, F.A. Villamena, J. Böker, R. Hardeland, M.A. Pappolla, B. Pucci, Amphiphilic amide nitrones: a new class of protective agents acting as modifiers of mitochondrial metabolism, J. Med. Chem. 53 (2010) 4849–4861.

[38] E. Jurado, M. Fernández-Serrano, F. Rios, M. Lechuga, Aerobic biodegradation of surfactants, in: Rolando Chamy (Ed.), Biodegradation, IntechOpen, 2013, pp. 63–81, , https://doi.org/10.5772/56120.

[39] M.J. Scott, M.N. Jones, The biodegradation of surfactants in the environment, Biochim. Biophys. Acta 1508 (2000) 235–251.

[40] C. Zou, X. Yan, Y. Qin, M. Wang, Y. Liu, Inhibiting evaluation of b-Cyclodextrin-modified acrylamide polymer on alloy steel in sulfuric solution, Corros. Sci. 85 (2014) 445–454.

[41] N.V. Novikov, K.A. Formirovsky, N.A. Bragina, A.F. Mironov, G.A. Anan'eva, V.V. Bykova, N.V. Usol'tseva, Synthesis and mesomorphism of cationic derivatives of meso-aryl-substituted porphyrins and their metal complexes, Mendeleev Commun. 20 (2010) 239–241.

[42] ASTM G1 Standard Practice for Preparing, Cleaning, and Evaluation Corrosion Test Specimens, http://www.cosasco.com/documents/ASTM_G1_Standard_Practice.pdf.

[43] M.J. Frisch, G.W. Trucks, H.B. Schlegel, G.E. Scuseria, M.A. Robb, J.R. Cheeseman, G. Scalmani, V. Barone, B. Mennucci, G.A. Petersson, H. Nakatsuji, M. Caricato,

X. Li, H.P. Hratchian, A.F. Izmaylov, J. Bloino, G. Zheng, J.L. Sonnenberg, M. Hada, M. Ehara, K. Toyota, R. Fukuda, J. Hasegawa, M. Ishida, T. Nakajima, Y. Honda, O. Kitao, H. Nakai, T. Vreven, J.A. Montgomery Jr., J.E. Peralta, F. Ogliaro, M. Bearpark, J.J. Heyd, E. Brothers, K.N. Kudin, V.N. Staroverov, R. Kobayashi, J. Normand, K. Raghavachari, A. Rendell, J.C. Burant, S.S. Iyengar, J. Tomasi, M. Cossi, N. Rega, J.M. Millam, M. Klene, J.E. Knox, J.B. Cross, V. Bakken, C. Adamo, J. Jaramillo, R. Gomperts, R.E. Stratmann, O. Yazyev, A.J. Austin, R. Cammi, C. Pomelli, J.W. Ochterski, R.L. Martin, K. Morokuma, V.G. Zakrzewski, G.A. Voth, P. Salvador, J.J. Dannenberg, S. Dapprich, A.D. Daniels, Ö. Farkas, J.B. Foresman, J.V. Ortiz, J. Cioslowski, D.J. Fox, Gaussian 09, Revision C.01, Gaussian, Inc., Wallingford CT, 2009.

[44] L.H. Abdel-Rahman, A.M. Abu-Dief, M.S.S. Adam, S.K. Hamdan, Some new nano-sized mononuclear Cu(II) Schiff base complexes: design, characterization, molecular modeling and catalytic potentials in benzyl alcohol oxidation, Catal. Lett. 146 (2016) 1373–1396.

[45] L.H. Abdel-Rahman, A.M. Abu-Dief, H. Moustafa, S.K. Hamdan, Ni(II) and Cu(II) complexes with ONNO asymmetric tetradentate Schiff base ligand synthesis, spectroscopic characterization, theoretical calculations, DNA interaction and antimicrobial studies, Appl. Organomet. Chem. 31 (2017) e3555.

[46] I.B. Obot, D.D. MacDonald, Z.M. Gasem, Density functional theory (DFT) as a powerful tool for designing new organic corrosion inhibitors. Part 1: an overview, Corros. Sci. 99 (2015) 1–30.

[47] A.E. Okoronkwo, S.J. Olusegun, O.O. Oluwasina, The inhibitive action of chitosan extracted from *Archachatina marginata* shells on the corrosion of plain carbon steel in acid media, Anti-Corros. Methods Mater. 62 (2015) 13–18.

[48] X. Zheng, S. Zhang, W. Li, L. Yin, J. He, J. Wu, Investigation of 1-butyl-3-methyl-1H-benzimidazolium iodide as inhibitor for mild steel in sulfuric acid solution, Corros. Sci. 80 (2014) 383–392.

[49] R. Fuchs-Godec, M.G. Pavlovic, Synergistic effect between non-ionic surfactant and halide ions in the forms of inorganic or organic salts for the corrosion inhibition of stainless-steel X4Cr13 in sulphuric acid, Corros. Sci. 58 (2012) 192–201.

[50] D.G. Duff, S.M.C. Ross, D.H. Vaughan, Adsorption form solution: an experiment to illustrate the Langmuir isotherm, J. Chem. Educ. 65 (1988) 815–816.

[51] H.M. Abd El-Lateef, A.M. Abu-Dief, L.H. Abdel-Rahman, E.C. Sañudo, N.N. Aliaga-Alcalde, Electrochemical and theoretical quantum approaches on the inhibition of C1018 carbon steel corrosion in acidic medium containing chloride using some newly synthesized phenolic Schiff bases compounds, J. Electroanal. Chem. 743 (2015) 120–133.

[52] H.M. Abd El-Lateef, A.M. Abu-Dief, B.E.D.M. El-Gendy, Investigation of adsorption and inhibition effects of some novel anil compounds towards mild steel in H_2SO_4 solution: electrochemical and theoretical quantum studies, J. Electroanal. Chem. 758 (2015) 135–147.

[53] H.M. Abd El-Lateef, A.M. Abu-Dief, M.A.A. Mohamed, Corrosion inhibition of carbon steel pipelines by some novel Schiff base compounds during acidizing treatment of oil wells studied by electrochemical and quantum chemical methods, J. Mol. Struct. 1130 (2017) 522–542.

[54] M.A. Migahed, H.M. Mohammed, A.M. Al-Sabagh, Corrosion inhibition of H-11 type carbon steel in 1 M hydrochloric acid solution by N-propyl amino lauryl amide and its ethoxylated derivatives, Mater. Chem. Phys. 80 (2003) 169–175.

[55] K.C. Emregul, M. Hayvali, Studies on the effect of a newly synthesized Schiff base compound from phenazone and vanillin on the corrosion of steel in 2 M HCl, Corros. Sci. 48 (2006) 797–812.

[56] A.A. Abdul Azim, L.A. Shalaby, H. Abbas, Mechanism of the corrosion inhibition of Zn anode in NaOH by gelatine and some inorganic anions, Corros. Sci. 14 (1974) 21–24.

[57] Y. Ji, B. Xu, W. Gong, Z. Zhang, Z. Jin, W. Ning, Y. Meng, W. Yang, Y. Chen, Corrosion inhibition of a new Schiff base derivative with two pyridine rings on Q235 mild steel in 1.0 M HCl, J. Taiwan Inst. Chem. Eng. 66 (2016) 301–312.

[58] N. Hilal, W.R. Bowen, L. Alkhatib, O.A. Ogunbiyi, Review of atomic force microscopy applied to cell interactions with membranes, Chem. Eng. Res. Des. 84 (2006) 282–292.

[59] G. Gece, The use of quantum chemical methods in corrosion inhibitor studies, Corros. Sci. 50 (2008) 2981–2992.

[60] H. Chadwick, R.D. Beck, Quantum state resolved gas–surface reaction dynamics experiments: a tutorial review, Chem. Soc. Rev. 45 (2016) 3576–3594.

[61] T. Koopmans, Über die zuordnung von wellenfunktionen und eigenwerten zu den einzelnen elektronen eines atoms, Physica 1 (1934) 104–113.

[62] H.B. Michaelson, The work function of the elements and its periodicity, J. Appl. Phys. 48 (1977) 4729–4733.

[63] I. Lukovits, E. Kalman, F. Zucchi, Corrosion inhibitors – correlation between electronic structure and efficiency, Corrosion 57 (2001) 3–8.

[64] R. Hariharaputhran, A. Subramanian, A.A. Antony, P. Manisankar, T. Vasudevan, S.V. Iyer, Influence of nitrones on corrosion inhibition and hydrogen permeation through mild steel in acidic solutions, Anti-Corros. Methods Mater. 46 (1999) 35–39.

[65] L.G. Qiu, Y. Wu, Y.M. Wang, X. Jiang, Synergistic effect between cationic gemini surfactant and chloride ion for the corrosion inhibition of steel in sulphuric acid, Corros. Sci. 50 (2008) 576–582.

[66] S.A. Umoren, O. Ogbobe, I.O. Igwe, E.E. Ebenso, Inhibition of mild steel corrosion in acidic medium using synthetic and naturally occurring polymers and synergistic halide additives, Corros. Sci. 50 (2008) 1998–2006.

[67] X. Wang, H. Yang, F. Wang, Inhibition performance of a gemini surfactant and its co-adsorption effect with halides on mild steel in 0.25 M H_2SO_4 solution, Corros. Sci. 55 (2012) 145–152.

[68] J. Hamer, A. Macaluso, Nitrones, Chem. Rev. 64 (1964) 473–495.